Pergamon

Int. J. Heat Mass Transfer. Vol. 40, No. 6, pp. 1411–1426, 1997

0017–9310/97 $17.00+0.00

PII: S0017–9310(96)00193–7

Effect of gravity modulation on natural convection in a vertical slot

Y. Y. JIN and C. F. CHEN

Department of Aerospace and Mechanical Engineering, The University of Arizona, Tuscon, AZ 85721, U.S.A.

(*Received* 11 *May* 1995 *and in final form* 17 *May* 1996)

Abstract—The effect of a sinusoidal gravity modulation on natural convection of fluids with constant property, in vertical slots of aspect ratio of 20 and 15, is studied numerically by a finite difference method. The gravity modulation is characterized by the nondimensional amplitude R_g and nondimensional frequency ω_f. We find a low frequency g-modulation has a strong effect on the fluid flow but little effect on the heat transfer rate. The flow of air usually enters a periodic state after two cycles of g-modulation, much faster than that of large Prandtl number fluids. The response is generally in the synchronous mode, except at $\omega_f = 10$ and $R_g = 1$ for air where it appears to be subharmonic. For a multicellular primary flow of air, g-modulation at $\omega_f = 25$ and $R_g = 1$ changes the multicellular primary flow to a unicellular one, demonstrating significant stabilizing effect. For high Prandtl number fluids, a flow pattern, consisting of horizontal secondary cells, preceded the onset of the commonly observed vertical secondary cells. At low modulation frequencies, stability of convection is enhanced as demonstrated by the increase in the critical Grashof number, by approximately 154% at $R_g = 1.6$ and $\omega_f = 40$. The temperature remains unchanged within the cycle of the modulation, totally different from the case of air, and gives a critical gradient approximately 0.56 at the center. Copyright © 1996 Elsevier Science Ltd.

1. INTRODUCTION

A laboratory in an orbiting spacecraft provides a unique micro-gravity environment for experimentation in fundamental studies in many fields of science, particularly in fluid physics and crystal growth. In such a micro-gravity environment, buoyancy-induced convection is expected to be minimized or to be absent, conditions favorable to the development of advanced materials. However, random fluctuations of the gravity field, both in magnitude and direction, experienced in the space laboratory (known as g-jitter) significantly influence the natural convection; for details, see a recent comprehensive review by Nelson [1].

For the Rayleigh–Bénard problem, Gresho and Sani [2] and Gershuni *et al.* [3] studied the effect of sinusoidal gravity modulation by linear stability theory. They found the system may be stabilized by gravity modulation, much in the same manner as an inverted pendulum may be stabilized by vertical oscillation. The instabilities may be in the synchronous or subharmonic modes. Biringen and Danabasoglu [4] studied the problem in a finite cavity by means of numerical integration of the two-dimensional, time-dependent Navier–Stokes equations. Their results are in good agreement with those of Gresho and Sani. Biringen and Peltier [5] extended the numerical methods to study the three-dimensional problem with sinusoidal or random gravity modulation. Clever *et al.* [6] performed a nonlinear analysis of the problem and found that finite-amplitude synchronous convection can be unstable to subharmonic modes. An experimental investigation was performed recently by Ishikawa and Kamei [7], who confirmed the theoretical prediction of possible enhancement of stability by gravity modulation.

Saunders *et al.* [8] studied the related problem of the effect of g-modulation on the stability of a double-diffusive layer. They found resonant instability with frequencies that are the multiples of the onset frequencies of the double-diffusive layer in the absence of modulation. Terrones and Chen [9] studied the added effect of cross-diffusion in such a system. They found bifurcating neutral curves with double minima, corresponding to the quasi-periodic mode and the subharmonic mode, respectively. As a consequence, at the critical Rayleigh number, there are two incommensurate critical wavenumbers at two incommensurate onset frequencies.

The effect of g-modulation on the convection in a square cavity by lateral heating was investigated by Ramachandran [10] using a finite-difference numerical simulation scheme. He found multicellular convection patterns that significantly affect the heat transfer characteristics. More recently, this problem was studied by Farooq and Homsy [11] using the method of perturbation expansion up to the second order. The expansion parameter ε is the amplitude of the g-modulation and it is assumed small, with the zeroth-order equation being the nonlinear Boussinesq equation in the absence of modulation. It was found that the streaming flow induced by the modulation, which was responsible for the multicellular flow pattern,

NOMENCLATURE

A	aspect ratio, H/L
g_0	terrestrial gravity
g_1	amplitude of the gravity modulation
Gr	Grashof number, $g\beta\Delta TL^3/\nu^2$
H	height of the slot
J	Jacobian derivative, $J(\omega,\psi) = \partial\psi/\partial y\partial\omega/\partial x - \partial\psi/\partial x\partial\omega/\partial y$
L	width of the slot
Nu	Nusselt number
Pr	Prandtl number, ν/α
Ra	Rayleigh number, $g\beta\Delta TL^3/\alpha\nu$
R_g	dimensionless amplitude of the gravity modulation, g_1/g_0
S	dimensionless vertical temperature gradient at the center, $\partial\theta/\partial y$
t	dimensionless time
T	temperature
x,y	dimensionless Cartesian coordinates
U	characteristic velocity, $g\beta\Delta TL^2/\nu$
u,v	dimenionless velocity components.

Greek symbols

α	thermal diffusivity
β	coefficient of volumetric expansion
ΔT	temperature difference
θ	dimensionless temperature
ν	kinematic viscosity
ρ	density
τ	phase angle of the gravity modulation, $\omega_f t$
ϕ	phase angle difference
ψ	stream function
ω	vorticity
ω_f	dimensionless frequency of the gravity modulation, $L^2\Omega/\nu$
Ω	frequency of the gravity modulation
∇^2	del operator $= \partial^2/\partial x^2 + \partial^2/A^2\partial y^2$.

Subscripts

c	cold wall or critical value
h	hot wall
L	local value
max	maximum value.

became appreciable when the Rayleigh number was large, thus affecting the heat transfer.

The effect of g-modulation on the stability of convection generated by lateral heat across a narrow, infinitely long slot was studied by Baxi *et al.* [12]. This is an attractive problem for stability analysis since the basic flow is known in closed form. By use of the Galerkin method, Baxi *et al.* reduced the linear stability problem to a system of simultaneous ordinary differential equations with periodic coefficients. The solution of the system was obtained by applying the Floquet theory. They found that, for a given frequency of oscillation, the stability is enhanced when the amplitude is small, but it is reduced at high amplitudes. Gershuni and Zhukhovitskii [13] studied the problem of g-modulation without a mean and with an arbitrary direction of the acceleration. They found that the system is most unstable when the direction of acceleration is perpendicular to the temperature gradient. Stability is enhanced as the direction of acceleration is tipped towards that of the temperature gradient, and the system becomes stable when the two directions coincide. Sharifulin [14] considered the problem of Baxi *et al.*, but limited the high modulation frequencies by considering the stability of averaged field equations. He found that, at sufficiently high frequency, the flow is unstable at any arbitrarily small mean values of g. In all these studies, no detailed parametric studies were made for small frequencies because of the large increase in computation time. However, it is the small-frequency gravity modulations that are found to influence most significantly the Rayleigh–Bénard convection and to have a larger effect on dopant concentration in the Bridgman–Stockbarger crystallization process [15]. Consequently, we undertake such a study in the present paper.

Under constant gravity, the natural convection in a vertical slot generated by a lateral temperature difference has been extensively studied analytically, experimentally and numerically in the past decades, see reviews by Bergholz [16], Lee and Korpela [17] and Le Quéré [18]. In detailed experimental studies, Elder [19] found the flow was in the conduction regime with a unicellular flow pattern at low Rayleigh numbers. When Ra exceeded a critical value, Ra_c, the unicellular convection became multicellular with secondary cells aligned in the vertical direction. In numerical studies, Lauriat and Desrayaud [20] found the critical Grashof number $Gr_c = 8900$ for air in a vertical slot with aspect ratio $A = 15$, Jin and Chen [21] obtained $Gr_c = 700$–720 at $Pr = 720$. Some of more recent reports on this problem are available in experiments by Chen and Wu [22] and Wakitani [23], and in numerical simulations by Daniels and Wang [24] and Jin and Chen [21]. Therefore one objective of this study is to make comparison between flows under constant gravity and under gravity modulation.

In this paper, a numerical simulation is carried out by solving the full non-linear equations to study in detail the effect of gravity modulation on natural convection of air and high Prandtl number fluids in ver-

tical slots with $A = 20$ for the former and 15 for the latter. The $A = 20$ was chosen because of our earlier steady g calculations [21] and $A = 15$ was chosen because of the apparatus for the planned experiments. We find the multicellular primary flow in the slot is significantly influenced by gravity modulation, especially at small frequencies.

The governing equations describing the flow and a numerical method are presented in Section 2. Extensive tests of the code developed based on the above method are followed in Section 3. In Section 4, detailed results are provided for air, including: effects of the frequency and amplitude of the gravity modulation on the multicellular primary flow, the increase of the critical Grashof number and the heat transfer result and for high Prandtl number fluids, including the flow development and the effect of primary flow. Finally some conclusions are presented in Section 5.

2. GOVERNING EQUATIONS AND NUMERICAL METHOD

Consider a vertical slot of height H and width L, with two horizontal impermeable, rigid adiabatic walls subject to a vertical sinusoidal gravity modulation $g_1\cos(\Omega t)$. The left and right walls are maintained at uniform constant temperatures, T_h and T_c ($< T_h$), respectively. The temperature difference is assumed to be small enough so that the Boussinesq approximation holds when a Newtonian fluid of density ρ, with constant kinematic viscosity ν and thermal diffusivity α, is contained in the cavity.

Assume the flow generated by the lateral temperature difference is two-dimensional. The governing equations can be nondimensionalized by: scaling the vertical coordinate by H, the horizontal coordinate by L, time by L^2/ν, temperature by $\Delta T = T_h - T_c$, velocity by $U = g\beta\Delta T L^2/\nu$, and pressure by ρU^2. By introducing the stream-function ψ and the vorticity ω

$$u = \frac{1}{A}\frac{\partial \psi}{\partial y} \quad v = -\frac{\partial \psi}{\partial x} \tag{1}$$

$$\omega = \frac{\partial v}{\partial x} - \frac{1}{A}\frac{\partial u}{\partial y} \tag{2}$$

we obtain the nondimensional governing equations:

$$\frac{\partial w}{\partial t} = -\frac{Gr}{A}J(\omega, \psi) + \nabla^2\omega + (1 + R_g\cos(\omega_f t))\frac{\partial \theta}{\partial x} \tag{3}$$

$$\nabla^2\psi = -\omega \tag{4}$$

$$\frac{\partial \theta}{\partial t} = -\frac{Gr}{A}J(\theta, \psi) + \frac{1}{Pr}\nabla^2\theta. \tag{5}$$

The boundary conditions are

$$x = 0 \quad \psi = \partial\psi/\partial x = 0 \quad \theta = 1 \tag{6}$$

$$x = 1 \quad \psi = \partial\psi/\partial x = 0 \quad \theta = 0 \tag{7}$$

$$y = 0 \quad \psi = \partial\psi/\partial y = 0 \quad \partial\theta/\partial y = 0 \tag{8}$$

$$y = 1 \quad \psi = \partial\psi/\partial y = 0 \quad \partial\theta/\partial y = 0. \tag{9}$$

The effect of the gravity modulation is clearly reflected in the buoyancy terms of equation (3).

A finite difference method is used to solve the above governing equations. We adopt the schemes by Lee and Korpela [17] to discretize equations (3) and (5), that is, the explicit scheme of Arakawa [25] for the nonlinear terms, the DuFort–Frankel [26] scheme for the diffusive terms (the time step should thus satisfy the Courant condition) and the central difference scheme for the time derivatives. The Poisson equation (4) is solved by the alternating direction implicit (ADI) method [27], aided with the prediction method [28] and block correction technique (BCT) [29]. The boundary vorticity is determined by Thom's rule [27].

3. ACCURACY ASSESSMENT

The code based on the above algorithm is fully tested. In the following, we present testing cases with constant gravity and with gravity modulation, and compare our results with known results:

(1) The test case with constant gravity. The natural convection of air in vertical slots is calculated. A detailed comparison at aspect ratio $A = 16$ and 20 can be found in Jin and Chen [21]. The following is a brief summary. For $A = 16$, we compared our results with those of the two-cell solution at $Ra = 24\,000$ ($Gr = 33\,803$) calculated by Le Quéré [18] using the Tau–Chebyshev algorithm. A grid convergence study showed that grids of 33×129 gave satisfactory results, within 3% of the results of Le Quéré even for the most sensitive quantity, the vorticity in the slot. The streamline showed a two-cell secondary flow pattern with a wavenumber of approximately 1.60 [21]. The flow pattern and the wavenumber agree very well with Le Quéré, who obtained a wavenumber of 1.59. For $A = 20$, we obtained the critical Grashof number $Gr_c = 8800$–8900, which was in excellent agreement with that predicted by Lauriat and Desrayaud [20], who obtained $Gr_c = 8900$.

(2) The test case with sinusoidal gravity modulation. We calculate the natural convection of water in a square cavity at $Ra = 1.88 \times 10^4$ under gravity modulation with $R_g = 10$ and $\Omega = 0.01$ Hz. The flow patterns, obtained with grids 33×33, in one cycle of the modulation are show in Fig. 1. These multicellular flow patterns are in good agreement with those obtained by Ramachandran [10] with grids 31×31. Compared with the case of constant gravity, the heat transfer rate is improved by 39.39%, which agrees almost exactly with Ramachandran, who obtained an improvement of 39.32% in the heat transfer rate.

4. RESULTS AND DISCUSSION

The natural convection of air and higher Prandtl number fluids in a vertical slot under gravity modu-

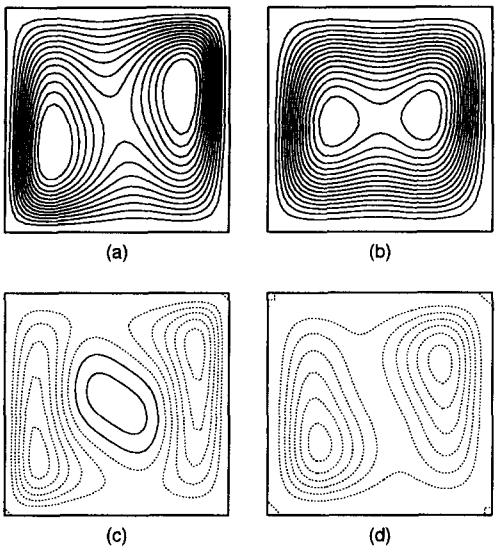

Fig. 1. Flow patterns of water at $Ra = 1.88 \times 10^4$, $A = 1$, $\Omega = 0.01$ Hz and $R_g = 10$ with $\Delta\psi = 7 \times 10^{-5}$. Solid and dotted lines denote $\psi < 0$, and $\psi > 0$, respectively: (a) t = 0; (b) $\pi/2$; (c) π; (d) $3\pi/2$.

lation is studied in detail. We chose $A = 20$ for air and $A = 15$ for large Prandtl number fluids, so as to compare the present study with cases of constant gravity. We note here that the results in this study are obtained based on grids of 33×129.

4.1. *Air in a vertical slot with* A = 20

First, the flow at $Gr = 10\,000$ with constant gravity is determined, which appears multicellular because the Grashof number is slightly larger than the critical value, $Gr_c = 8800$–8900. The six weak secondary cells have an average wavelength of $2.28L$ (Fig. 2(a)). The isotherm shows slightly convective motion, corresponding to the weak secondary cells (Fig. 2(b)). Based on this multicellular primary flow, we study the effects of the frequency and amplitude of the gravity modulation on the flow. Furthermore, based on the periodic primary flow at parameter set of $\omega_f = 25$ and $R_g = 1$, we determine the critical Grashof number.

4.1.1. *Effect of frequency.* We keep $Gr = 10\,000$ and nondimensional amplitude $R_g = 1$. The nondimensional frequency ω_f of the gravity modulation varies from 10 to 800, corresponding to a physical frequency range $\Omega = 0.25$–20 Hz for a slot with width 1 cm. When adding the gravity modulation, we find the flow enters the periodic state quite quickly: only two cycles of modulation are usually required.

The temperature response at periodic state in three cycles of gravity modulation at $\omega_f = 10$ is shown in Fig. 3. In this figure PA, PB and PC are sampling points located at the nondimensional coordinate points (0.25, 0.50), (0.25, 0.75) and (0.50, 0.75), respectively. Figure 3 reveals that the temperature response at $\omega_f = 10$ requires two cycles of modulation to repeat itself completely. This indicates that the response is in the subharmonic mode. The flow patterns in two cycles of periodic state are shown in Fig. 4. We note here that the increase of streamfunction is $\Delta\psi = 4 \times 10^{-5}$ only at the phase angle $\tau = \pi$ and 3π; it is smaller than $\Delta\psi = 40 \times 10^{-5}$ at other phase angles, in order to visualize the flow pattern. We also note that the phase angle τ is expressed in a relative value for simplicity, instead of the exact value in the modulated gravity. As can be seen, the flow is very strong at $\tau = 0 - \pi/2$ and very weak at $\tau = \pi - 3\pi/2$ of the modulation. It can be unicellular at $\tau = 0$ and $3\pi/2$, or multicellular with six secondary cells at $\tau = \pi/2$ and

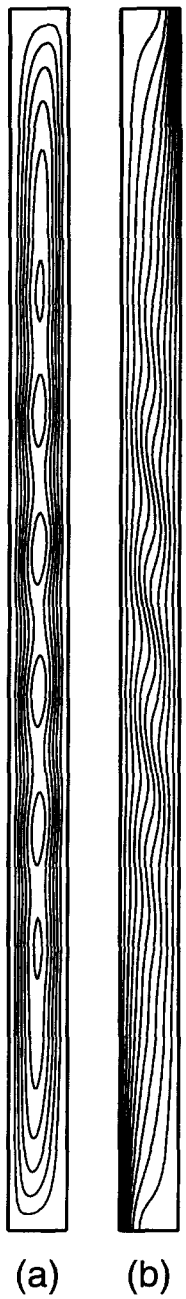

Fig. 2. Flow pattern of air and isotherms at $Gr = 10\,000$ and $A = 20$ with constant gravity: (a) flow pattern with $\Delta\psi = 40 \times 10^{-5}$; (b) isotherm.

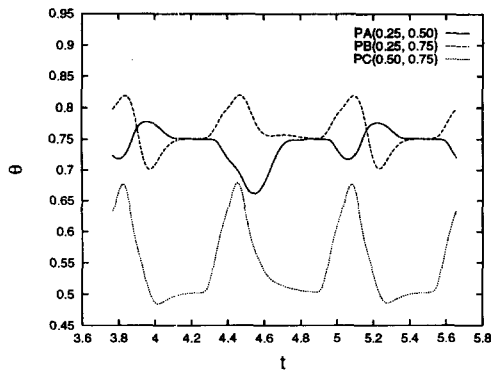

Fig. 3. Temperature response at sampling points PA, PB, PC at $Gr = 10\,000$, $\omega_f = 10$ and $R_g = 1$.

π, indicating that multicellular primary flow can be stabilized or become stronger under the gravity modulation. The flow patterns in the second cycle are similar. However, there are seven secondary cells when the flow appears multicellular. The wavelengths are approximately $2.22L$, the same as the primary flow, in the first cycle and they decrease slightly to $1.83L$ in the second cycle. This variation in flow patterns confirms the subharmonic response of temperatures as shown in Fig. 3. The corresponding isotherms clearly exhibit straight lines at $\tau = 0$ and $3\pi/2$ and convective motion (similar to Fig. 2(b)) at $\tau = \pi/2$, in accordance with the dominant unicellular or multicellular flows in the slot.

The effect of gravity modulation at $\omega_f = 25$ is shown in Fig. 5. The flow shows unicellular patterns only in a whole cycle of the modulation and is weakest at $\tau = \pi$. The isotherms are shown in Fig. 5(b). They are straight lines within the cycle, in conformity with the unicellular flow patterns. This indicates that the multicellular primary flow is stabilized notably by the gravity modulation with $\omega_f = 25$ and $R_g = 1$.

The flow at higher frequency modulation is mainly multicellular with a wavelength close to the primary flow, which need not be repeated here for the sake of brevity. Therefore, it is low frequency modulation that shows a notable effect on the multicellular primary flow.

4.1.2. *Effect of amplitude.* Keeping the nondimensional frequency $\omega_f = 25$ and $Gr = 10\,000$, we change the amplitude of the modulation from $R_g = 0.5$, to 1.5. The flow at $R_g = 0.5$ is mainly multicellular with a constant wavelength $2.18L$. The isotherms show convective motion. The flow patterns at $R_g = 1.5$ are shown in Fig. 6(a); they are mainly multicellular with a wavelength $2.67L$. Therefore, the wavelength is slightly increased with an increase of the amplitude of the gravity modulation. The multicellular flow is very strong at $\tau = \pi/2$, and very weak at $\tau = \pi$ and $3\pi/2$. It is counterrotating at $\tau = \pi$ because of the negative value of the gravity, but has the same wavelength. The isotherms are shown in Fig. 6(b). They show straight lines at $\tau = 0$, and strong convective motion at $\tau = \pi/2$. The effect of the counterrotating flow on the isotherms is clearly shown at the ends of the slot, at $\tau = \pi$ and $3\pi/2$. Comparing the flow pattern and isotherm at $t = 3\pi/2$, we can see the response of the temperature is delayed, the temperature still exhibits the influence of the counterrotating flow.

Therefore, for a specific frequency of the modulation, e.g. $\omega_f = 25$, there is an amplitude range, e.g. close to $R_g = 1$, with which the multicellular primary flow can be notably stabilized by the gravity modulation. The large amplitude modulation will make the multicellular flow remarkably stronger. This conclusion is qualitatively in agreement with that by Baxi *et al.* [12] in their linear stability analysis. They found that the critical Grashof number decreases with larger amplitude modulation. However, a small amplitude modulation does not demonstrate a significant stabilizing effect on the multicellular primary flow.

4.1.3. *Critical Grashof number at* $\omega_f = 25$ *and* $R_g = 1$. Since the gravity modulation at $\omega_f = 25$ and $R_g = 1$ significantly stabilizes the multicellular primary flow, as shown in the above sections, we chose this case to determine the critical Grashof number. We begin the calculation from an initially motionless state. Calculations at higher Grashof numbers are started from the result of lower Grashof numbers with gravity modulation. Therefore the primary flow is periodic and unicellular.

The flow usually enters the periodic state after only two cycles of modulation. The periodic flow is unicellular in the entire cycle. The flow patterns and isotherms at $Gr = 10\,000$ are the same as in Fig. 5, which implies the flow type of the primary flow, periodically unicellular primary flow or stably multicellular primary flow, has little effect on the final state for thermal convection of air with $Pr = 0.71$. This result is completely different from the cases of large Prandtl number fluids, as presented in Section 4.2.

When the Crashof number increases to 12 000 from 10 000, multicellular flow patterns are found at $\tau = \pi/2$ and π, as shown in Fig. 7(a). The corresponding isotherms are given in Fig. 7(b). They show straight lines or convective motion, in accordance with the flow patterns. Therefore the critical Grashof number for the periodic primary flow increases to $Gr_c = 10\,000$–$12\,000$, which is about 23.6% higher than that with constant gravity.

The horizontal velocity and temperature profiles at $Gr = 10\,000$ and 12 000, just before and after the onset of the instability, are shown in Figs 8–9. At $Gr = 10\,000$, the horizontal velocity shows wave-like variation in whole cycle. Such wavy variation is notable at the nondimensional heights about $y = 1/5$ and 4/5. This implies that the instability will not occur around the central zone as observed in cases with constant gravity. A smaller increase of the stream function does visualize some small, weak secondary cells, which is in accordance with the negative and positive values of the horizontal velocity at heights

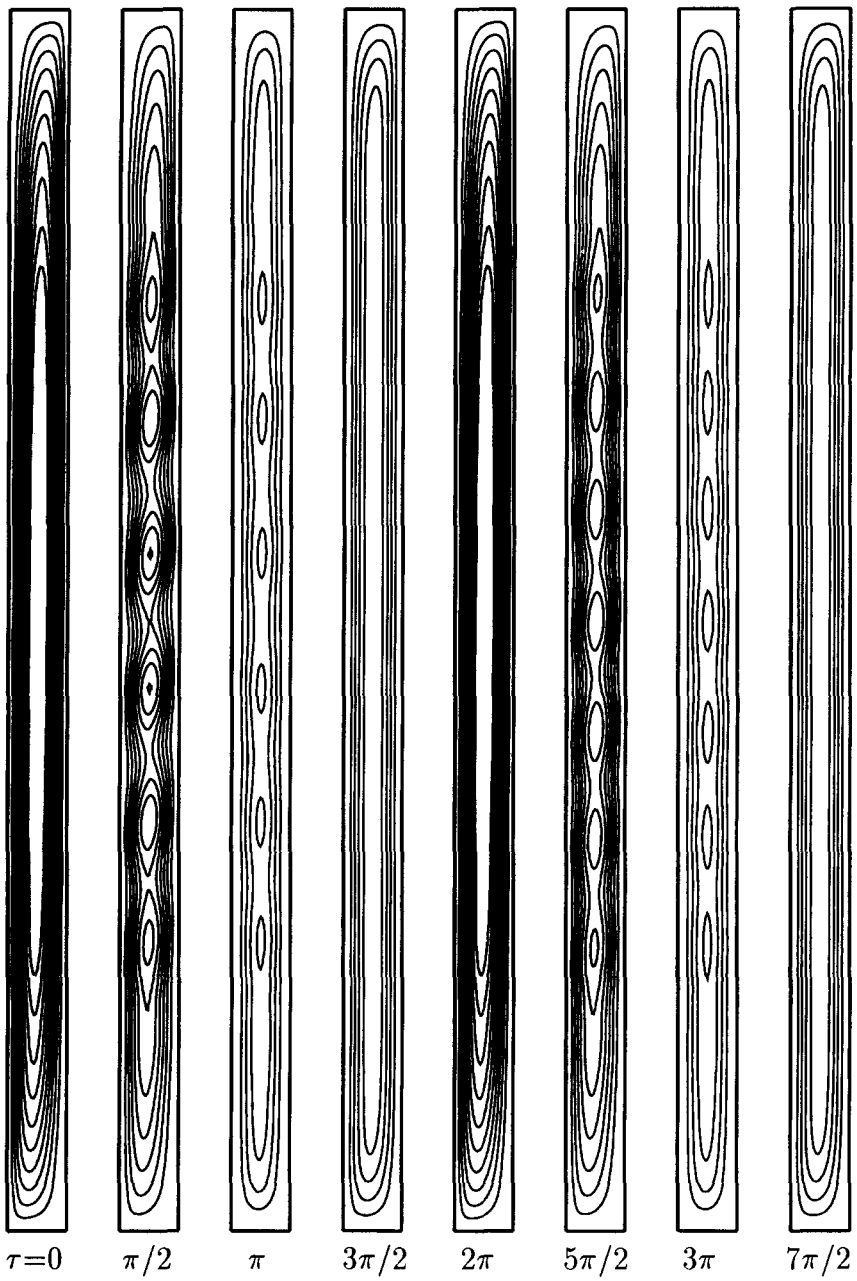

Fig. 4 Flow patterns with $\Delta\psi = 40 \times 10^{-5}$ except at time $t = \pi$ and 3π (with $\Delta\psi = 4 \times 10^{-5}$ only) at $Gr = 10\,000$, $\omega_F = 10$ and $R_g = 1$.

around $y = 1/4$ and $3/4$. The temperature profiles show large variation in the upper and lower center regions, as shown in Fig. 8(b) at $Gr = 10\,000$, within the cycle of the modulation. It is clear from Fig. 8 that the temperature gradient at the center varies during the cycle of the modulation. Wavy variation of the temperature is located around the heights $y = 1/4$ and $3/4$, in agreement with the variation of the horizontal velocity. After the onset of the secondary cells at $Gr = 1200$ large wave-like variations of the horizontal velocity and temperature are developed, as shown in Fig. 9. The regular waviness of the velocity in the center region is similar to cases of constant gravity. The large waviness is in accordance with the visible secondary cells in the slot, as shown in Fig. 7(a). The variation of the velocity in the end regions is close to the case of $Gr = 10\,000$. The wavelike variation of the temperature is also similar to cases with constant gravity and varies during the cycle of the modulation. The temperature increases inside the secondary cells and decreases between the cells along the height. Its largest modulation at $\tau = \pi$, corresponding to the dotted line C in Fig. 9(b), agrees with the weak secondary cells as shown in Fig. 7(a), because the weak secondary flow cannot mix the fluid thoroughly to weaken the temperature gradient.

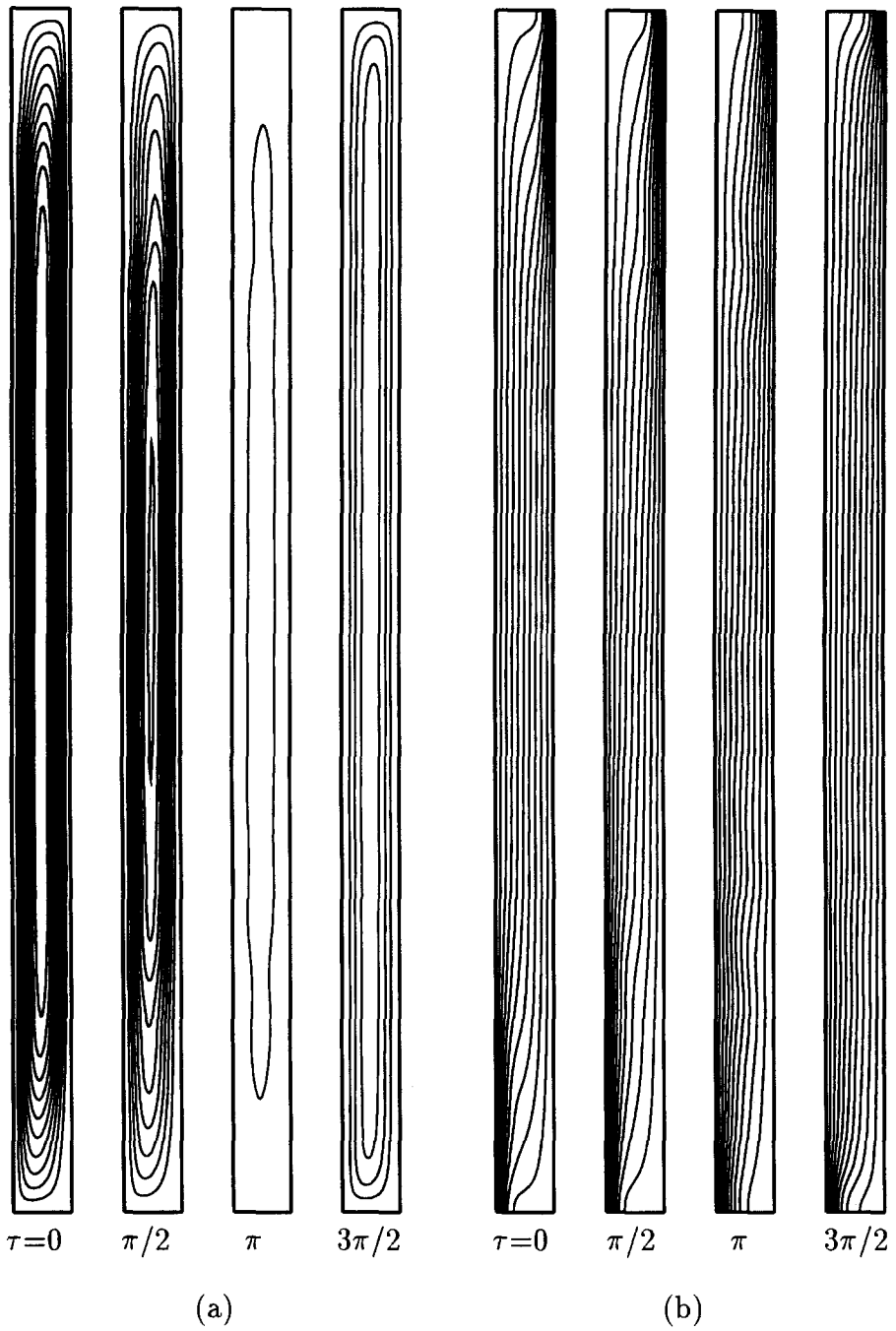

Fig. 5. Flow patterns and isotherms at $Gr = 10000$, $\omega_f = 25$ and $R_g = 1$: (a) flow patterns with $\Delta\psi = 40 \times 10^{-5}$; (b) isotherms.

4.1.4. *Heat transfer results.* The local heat transfer rate along any vertical plane in the cavity is given by

$$Nu_L = -\frac{\partial\theta}{\partial x} + Pr\,Gr\,u\theta. \tag{10}$$

It shows large variation at the end regions during the cycle. It also shows smaller wave-like variations at heights around $y = 1/4$ and $3/4$, before the onset of the secondary cells, in accordance with the horizontal velocity and temperature variations as shown in Fig. 8. With development of the secondary cells, the local heat transfer rate shows notably wavy variation. The maximum value of the wavy Nusselt number is located in the lower part of the secondary cell, while the minimum value is in the top of the secondary cell. They are in agreement with the variation of isotherms as shown in Fig. 7(b).

The average heat transfer rate, Nu_t at the hot wall is calculated by Simpson's rule. It varies with time, and usually appears periodic after one cycle of modulation

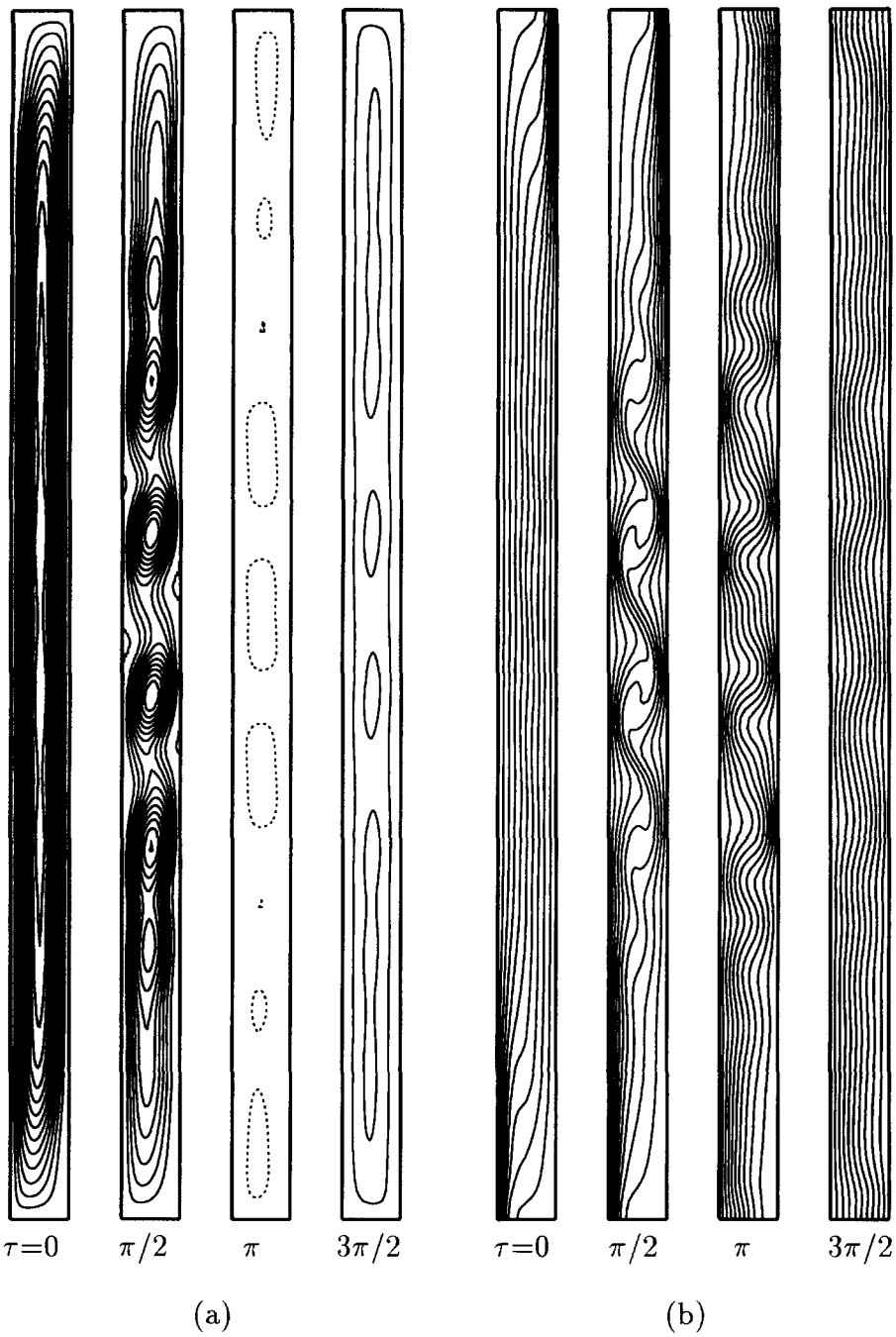

Fig. 6. Flow patterns and isotherms at $Gr = 10000$, $\omega_f = 25$ and $R_g = 1.5$: (a) flow patterns with $\Delta\psi = 40 \times 10^{-5}$—dotted lines denote $\psi > 0$; (b) isotherms.

only. Its amplitude decreases with increase of the frequency and increases with the amplitude of the gravity modulation. The peak values of Nu_t are postponed compared with the peaks of the gravity. The phase angle differences, ϕ_1 or ϕ_2, between the maximum or minimum values of Nu_t and the gravity, increase with the frequency of the modulation, as show in Fig. 10 for the multicellular primary flow at $Gr = 10000$ and $R_g = 1$. The variation of Nu_t is unsymmetric within the cycle, and the unsymmetric degree (ϕ_3) phase angle difference between the maximum and minimum Nu_t, is shown in Fig. 10. It has a maximum value at $\omega_f = 50$, and approaches zero when the frequency ω_f is larger than 400.

The heat transfer rate, Nu, in one or two cycles of the gravity modulation is an average value of Nu_t. We find that although the gravity modulation has a strong effect on the flow patterns, it shows little effect on the average heat transfer rate Nu. For $Gr = 10000$ with multicellular primary flow, the variation of the aver-

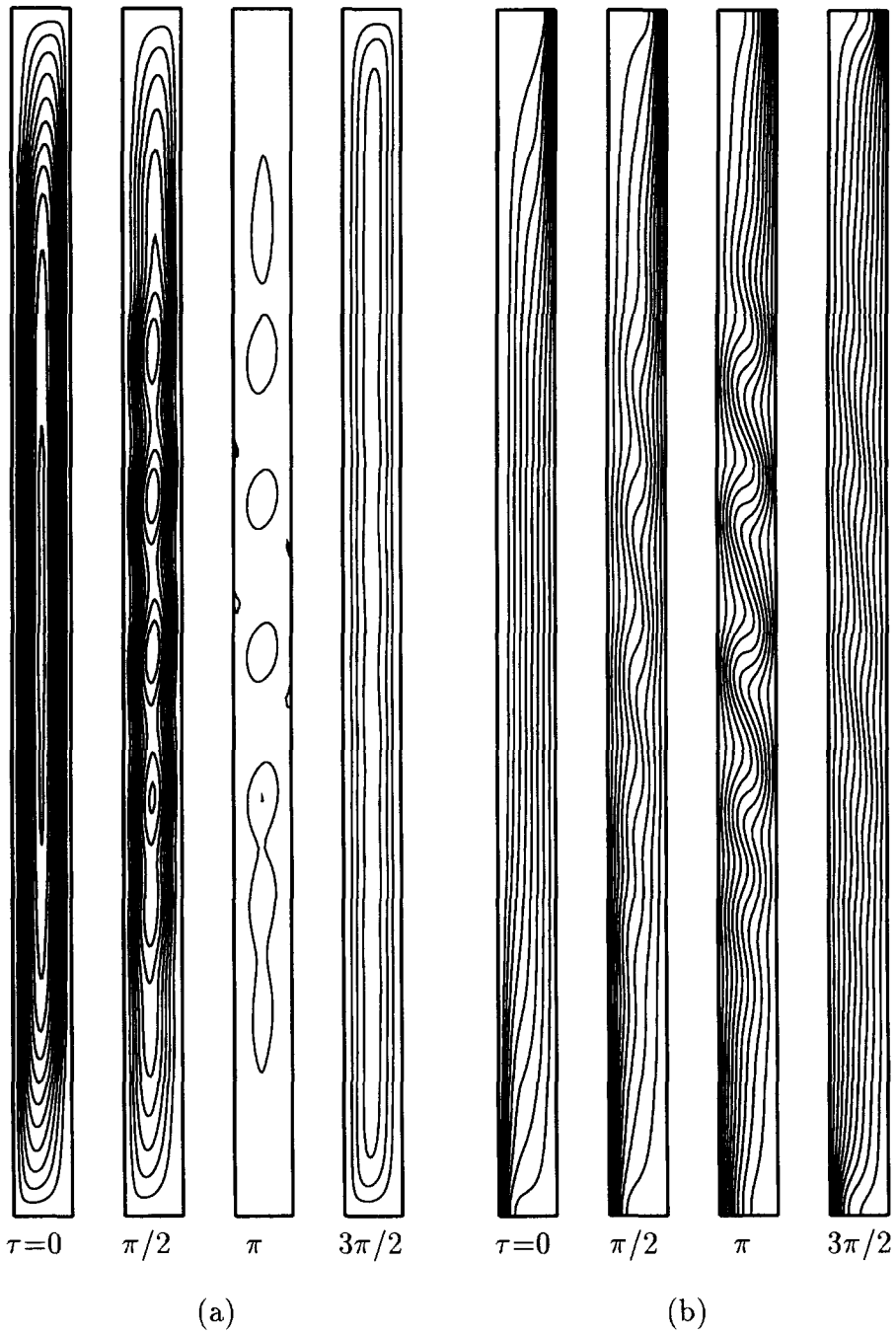

Fig. 7. Flow patterns and isotherms at $Gr = 12000$, $\omega_f = 25$ and $R_g = 1$: (a) flow patterns with $\Delta\psi = 40 \times 10^{-5}$; (b) isotherms.

age heat transfer rate Nu is less than 2% compared with the case of constant gravity.

4.2. *Fluids of large Prandtl number in a vertical slot of* A = 15

Based on linear stability analysis, Baxi *et al.* [12] found that large Prandtl number fluids have the potential to improve greatly the critical Grashof number, compared with small Prandtl number fluids, e.g. air. We focus our interest in determining the critical Grashof number for the onset of the convective instability. We find that before the onset of the typical multicellular flow, as in the case with constant gravity, the flow shows a different flow pattern, secondary cells aligned in the horizontal direction. Moreover, the effect of the initial flow condition on the final flow pattern is studied.

4.2.1. *Flow development at* Pr = 720, $R_g = 0.9$ *and* $\omega_f = 30$. We start the calculation from an initially motionless state. Calculations at higher Grashof num-

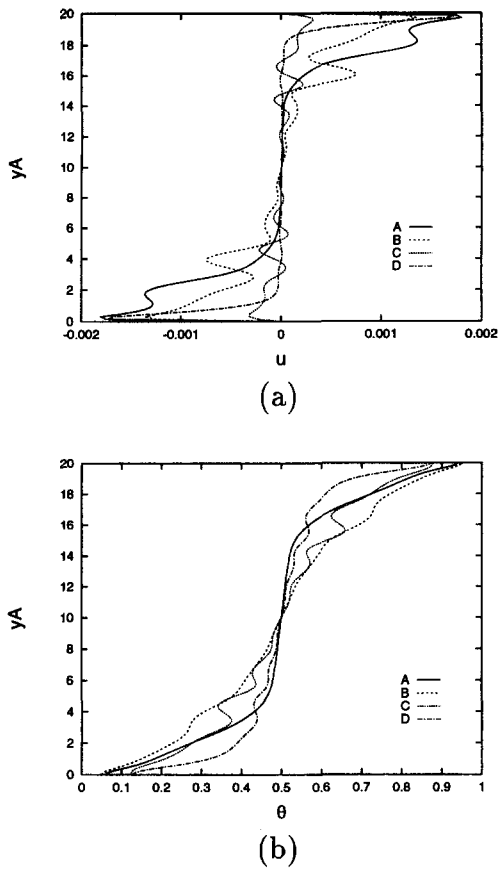

Fig. 8. Typical variations of the horizontal velocity, and temperature along the vertical central line at $Gr = 10\,000$ in one cycle of the gravity modulation. Lines A, B, C, and D are at $\tau = 0$, $\pi/2$, π, and $3\pi/2$: (a) horizontal velocity; (b) temperature.

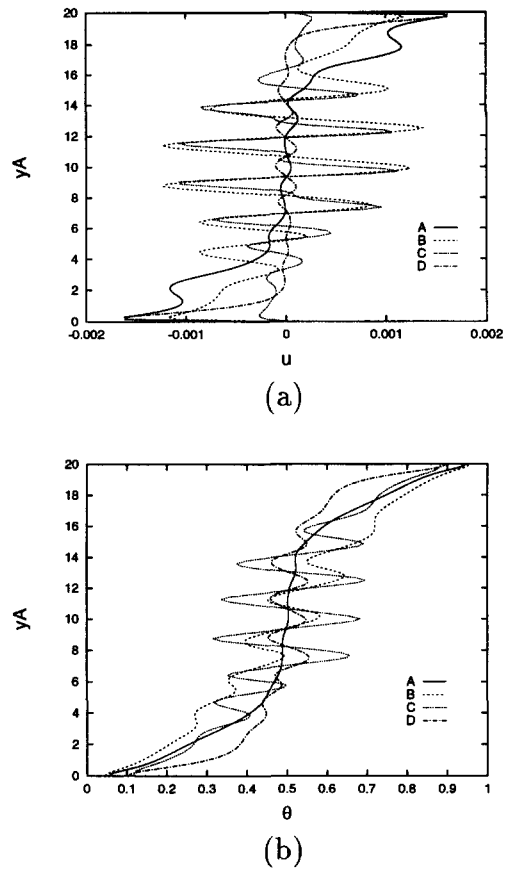

Fig. 9. Typical variations of the horizontal velocity, and temperature along the vertical central line at $Gr = 12\,000$ in one cycle of the gravity modulation. Lines A, B, C, and D are at $\tau = 0$, $\pi/2$, π, and $3\pi/2$: (a) horizontal velocity; (b) temperature.

ber are started from the results at lower Grashof number, namely periodic flow. The Prandtl number $Pr = 720$ corresponds to a 90% glycerin–water solution [30], the nondimensional frequency $\omega_f = 30$ corresponding to $\Omega = 1.5$ Hz for a slot with width 1.5 cm. We note that initially different results at a lower Grashof number, e.g. results at $\tau = 0$, $\pi/2$, π or $3\pi/2$ within the cycle of the modulation, finally give the same results. We find that the flow usually requires more than 30 cycles of the modulation to appear periodic.

The flow shows the boundary layer regime at a small Grashof number, $Gr = 100$. The typical flow patterns within one cycle of the modulation are show at Fig. 11(a) $Gr = 400$. The flow is unicellular, and strong in the first-half cycle and weak in the second-half cycle. Moreover, the streamline at the end of the central core shows concave feature towards the center at $\tau = 3\pi/2$. The corresponding isotherms are almost the same within the cycle (Fig. 11(b)), and indicate the typical boundary layer feature as in the case of constant gravity. As the Grashof number increases, the concavity of the central streamline becomes more salient. Finally, two parallel layers completely separated are formed, as shown in Fig. 12 at $Gr = 600$ and $\tau = 3\pi/2$. These secondary cells aligned in the horizontal direction are termed horizontal secondary cells. Such a flow pattern emerges periodically and exists briefly within the cycle of the gravity modulation. The streamline at the center at $\tau = 0$ also appears concave. The flow within the cycle is mainly

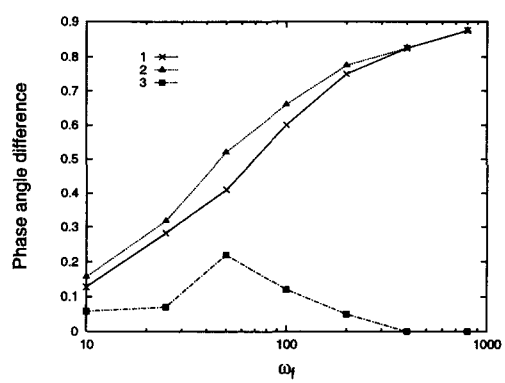

Fig. 10. Phase differences. 1—ϕ_1, between maximum Nu_t and gravity; 2—ϕ_2, between minimum Nu_t and gravity; 3—ϕ_3, unsymmetry of response of Nu_t.

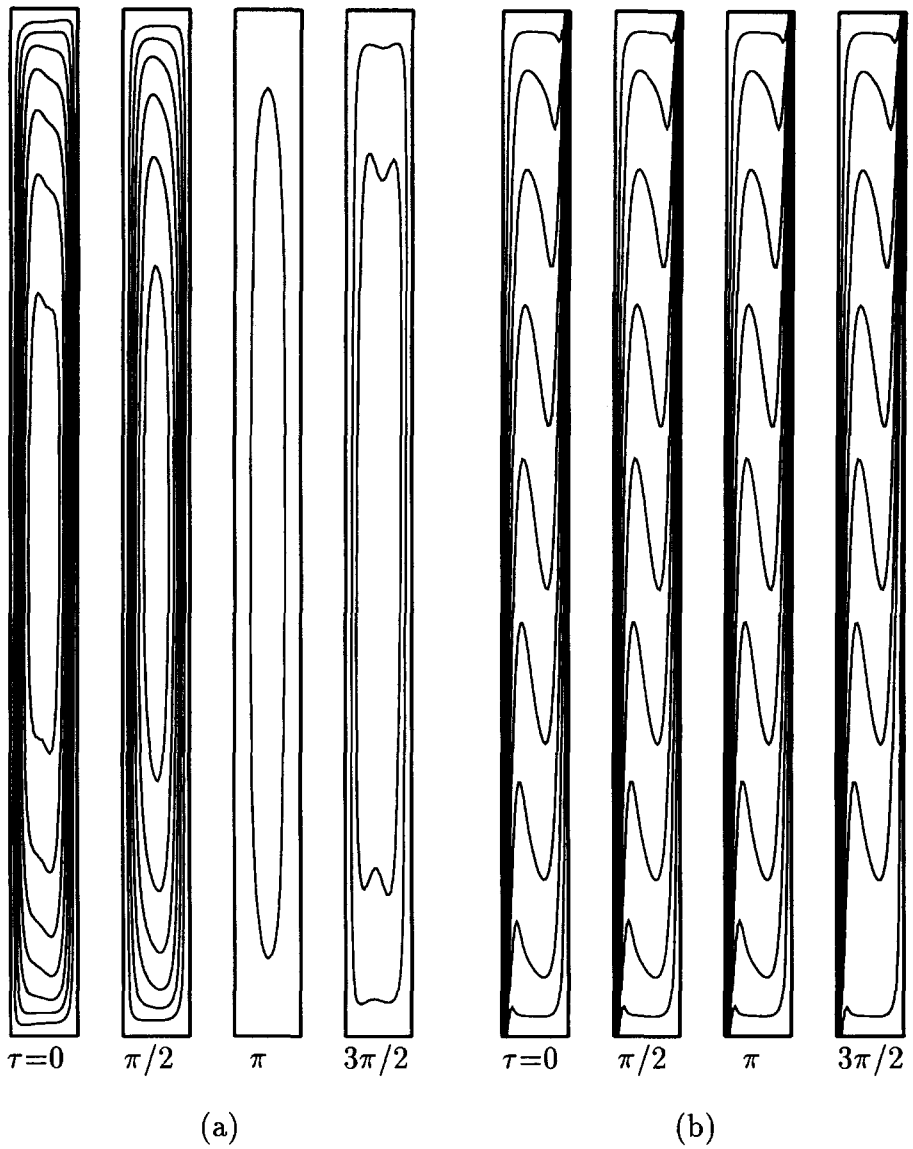

Fig. 11. Flow patterns and isotherms at $Gr = 400$, $Pr = 720$, $\omega_f = 30$ and $R_g = 0.9$: (a) flow patterns with $\Delta\psi = 8 \times 10^{-5}$; (b) isotherms.

unicellular. The isotherms are similar to Fig. 11(b). The increase of the Grashof number makes the horizontal cellular flow stronger, as shown in Fig. 13 at $Gr = 1200$. At $\tau = 0$, the flow shows two horizontal secondary cells almost totally separated. This indicates that the horizontal cellular flow not only becomes stronger, but also remains for a longer time within the cycle with an increase of the Grashof number. However, the isotherms do not show significant change with the increase of the Grashof number. As the Grashof number is further increased $Gr = 1400$, typical secondary cells aligned in the vertical direction and therefore called vertical secondary cells, similar to the cases without gravity modulation, are found, as shown in Fig. 14, while the horizontal cells now disappear. The flow is multicellular in the whole cycle, and strong in the first-half cycle and weak in the second. If a smaller increase of the stream function is used to visualize the flow pattern, we find the flow keeps seven secondary cells and has several tertiary cells as shown at $\tau = 0$ of Fig. 14(a). The isotherms are almost unchanged during the cycle, and show strong convective motion, as presented in Fig. 14(b).

Therefore, the critical Grashof number is improved from $Gr_c = 700$–720 for the constant gravity case to $Gr^g_{cv} = 1200$–1400 by the gravity modulation, an approximate increase of 83%. Here the suffix 'g' denotes the gravity modulation, and 'v' denotes cells aligned in the vertical direction. Such a notable increase in the critical Grashof number is in accordance with the linear stability analysis. Moreover, we find horizontal secondary cells are formed at Gr^g_{ch} 400–600, and remain until the onset of the typical vertical

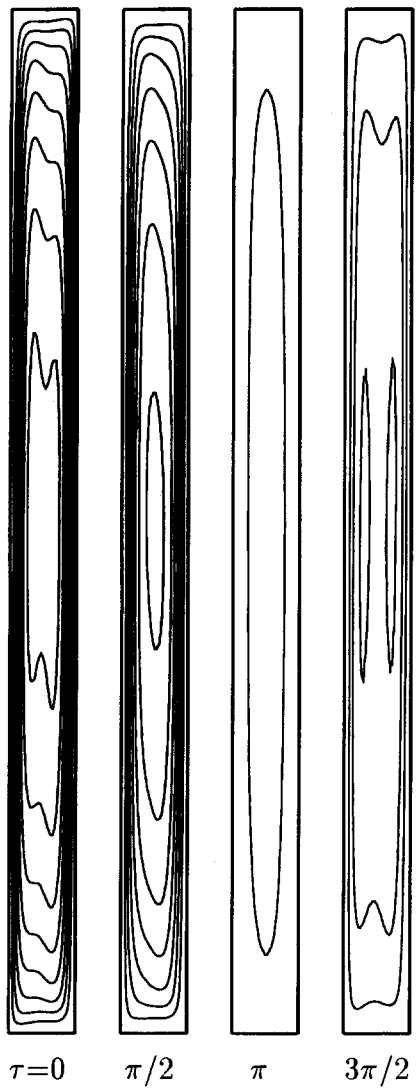

Fig. 12. Flow patterns with $\Delta\psi = 5.5 \times 10^{-5}$ at $Gr = 600$, $Pr = 720$, $\omega_f = 30$ and $R_g = 0.9$.

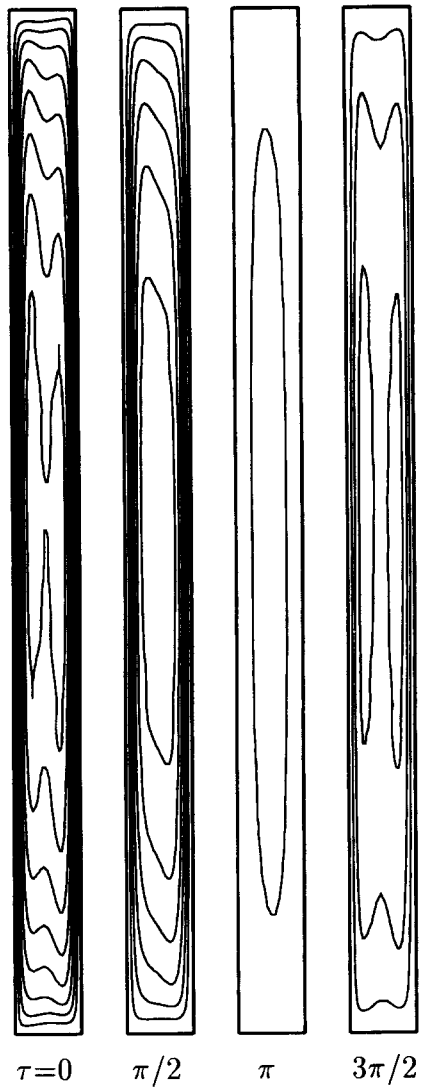

Fig. 13. Flow patterns with $\Delta\psi = 3.5 \times 10^{-5}$ at $Gr = 1200$, $Pr = 720$, $\omega_f = 30$ and $R_g = 0.9$.

secondary cells at Gr^g_{cv}. Such a flow pattern is not observed for the air, as presented in the Section 4.1, but this is not exceptional in this case. In our extensive studies, we find similar horizontal cells, for instance, at $Pr = 125$ and $A = 15$, as well as $Pr = 188$ and $A = 20$.

The typical profiles of horizontal velocity along the vertical central line are show in Fig. 15(a) at $Gr = 1200$. They vary within the cycle of the modulation, and show waviness, particularly at non-dimensional heights $y = 1/3$ and $2/3$, where the instability is developed first, instead of at the center. When the vertical secondary cells are developed, the profiles show large modulation. The temperature profiles are shown in Fig. 15(b) at $Gr = 1200$ and 1400. We note that the temperature profiles at $\tau = 0$, $\pi/2$, π and $3\pi/2$ at the specific Grashof number are located exactly on the same line. After the onset of the secondary cellular flow, the temperature shows step variation along the height, but still keeps unchanged within the whole cycle of the modulation. This feature of the temperature profile implies that the temperature gradient at the center keeps a constant during the cycle and is approximately 0.56 just before the onset of the secondary cells. We note that the temperature gradient is calculated based on the temperatures at the heights of $y = 0.25$ and 0.75. This feature is totally different from that in the case of air, in which the temperature profile varies within the cycle of the modulation.

At the mid-height of the slot, the vertical velocity shows negative and positive values at the central region at $\tau = 0$ and $3\pi/2$, in accordance with the two horizontal secondary cells shown in Fig. 13. However, the value of the velocity in the center is very small throughout the whole cycle, indicating that the flow is very weak in the central zone of the slot. The temperature profile at the mid-height is also unchanged during the cycle. At smaller Grashof numbers, the temperature shows a reversal gradient in the central

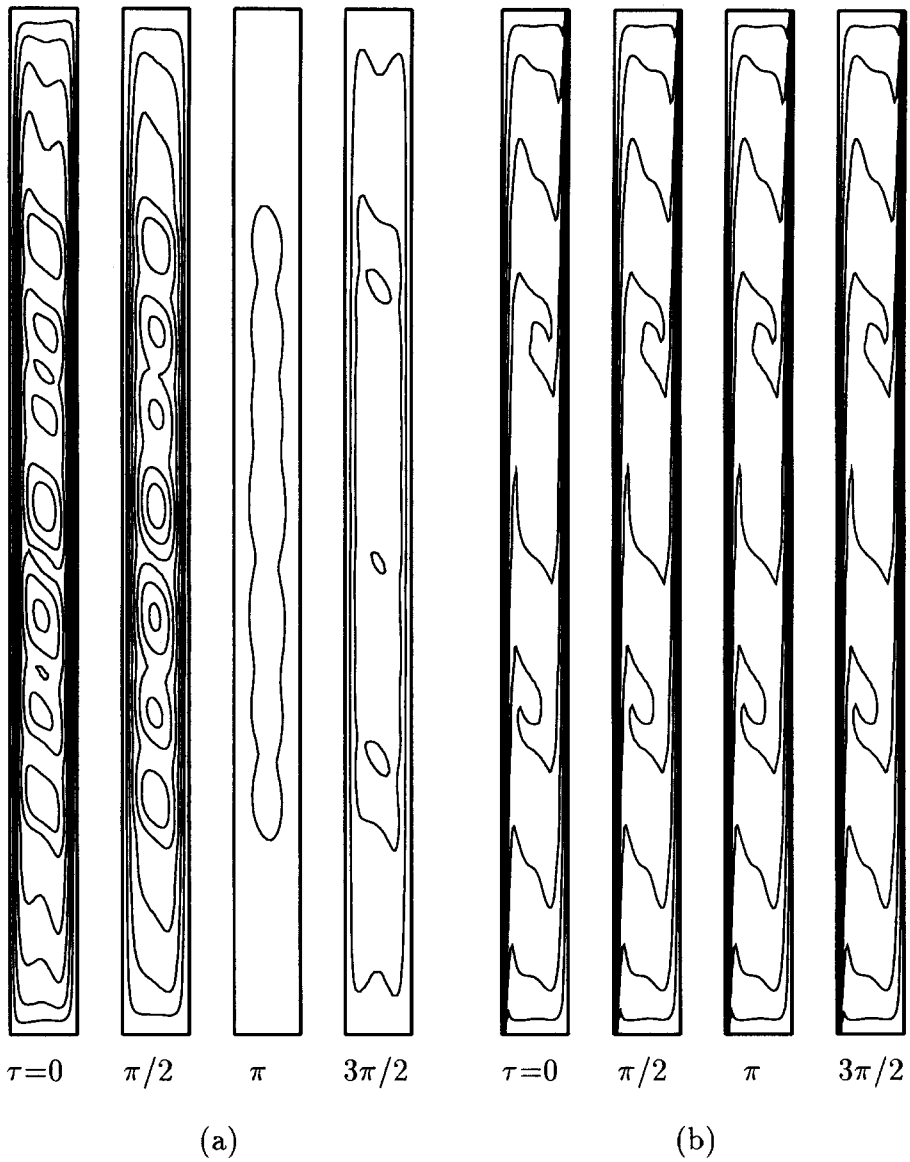

Fig. 14. Flow patterns and isotherms at $Gr = 1400$, $Pr = 720$, $\omega_f = 30$ and $R_g = 0.9$: (a) flow patterns with $\Delta\psi = 4.4 \times 10^{-5}$; (b) isotherms.

core. At higher Grashof numbers, e.g. $Gr = 1400$, the reversal temperature gradient disappears, and the temperature remains constant at approximately 0.51 in the core region. Such a temperature profile is similar to the case with constant gravity. Combining the isotherms shown in Figs. 11(b) and 14(b), it is clear that the temperature field in the slot is almost unchanged during the cycle of the modulation. This feature should be attributed to the effect of a large Prandtl number.

Because the temperature distribution is unchanged within the cycle of the modulation, the local heat transfer rate, Nu_D, along the hot wall does not vary during the cycle, in complete contrast for the case of air. The average heat transfer rate Nu within the cycles is almost the same as that in cases of constant gravity. Therefore the heat transfer rate is very insensitive to the gravity modulation, in the parameter range of the present study.

4.2.2. *Effect of the primary flow.* In the calculations above, we start the calculations from the results of low Grashof number under gravity modulation. The primary flow is therefore periodic and unicellular flow. We find that the type of primary flow has a strong effect on the final flow patterns of large Prandtl number fluids, while it has little effect on the flow of air.

We calculate the case of $Gr = 600$ and 800 with gravity modulation, based on the result of the same Grashof number without gravity modulation. The primary flow is thus unicellular in the former case and multicellular in the latter because $Gr_c = 700$–720 for cases with constant gravity. When acted upon with gravity modulation, the flow appears periodic, and finally shows two vertical cells at $Gr = 600$, as shown

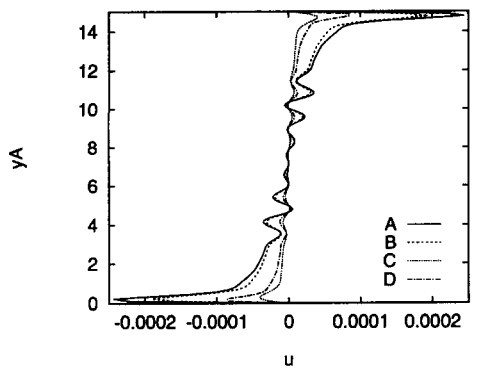

(a)

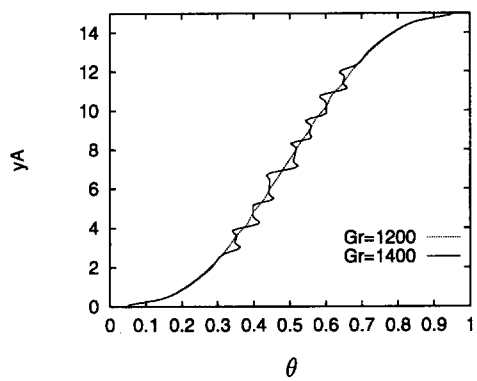

(b)

Fig. 15. Typical variations of the horizontal velocity, and temperature along the vertical central line in one cycle of the gravity modulation. Lines A, B, C, and D are at $\tau = 0$, $\pi/2$, π and $3\pi/2$: (a) horizontal velocity at $Gr = 1200$; (b) temperature at $Gr = 1200$ and 1400.

in Fig. 12. For $Gr = 800$, the flow remains multicellular, although it is strengthened or weakened within the cycle of the modulation (Fig. 16(a)). These flow patterns are totally different from those obtained from a periodically unicellular primary flow, which are very close to Fig. 12. The isotherms are also completely different, and show strong convective motion (Fig. 16(b)).

4.2.3. *Flow development at other parameter set.* The flow development at other parameters of amplitude and frequency of the modulation is studied at $Pr = 720$. The horizontal secondary cells are always found before the onset of the typical secondary cells. For $R_g = 0.1$, $\omega_f = 10$ and $R_g = 1.6$, $\omega_f = 40$, corresponding to physical frequencies of approximately 0.5 and 2.0 Hz, respectively; we obtained Gr_{cv}^{g} = 1000–1200 and 1700–1900, respectively. The more notable increase of the critical Grashof number at $R_g = 1.6$ and $\omega_f = 40$ should be attributed to a little large amplitude and still small frequency. The critical temperature gradient S at the center is found to be 0.55 and 0.57, respectively, for $R_g = 0.1$, $\omega_f = 10$ and $R_g = 1.6$, $\omega_f = 40$.

The flow development at $Pr = 125$ with $R_g = 0.9$, $\omega_f = 160$ is similar. The increase of the critical Grashof number is very small. The critical temperature gradient S is approximately 0.55, very close to the values presented above. Therefore, for a slot of $A = 15$, the critical temperature gradient has almost a constant value of 0.56 on average. This value is slightly higher than that obtained in cases without gravity modulation, namely $S = 0.49$ presented by Jin and Chen [21].

5. CONCLUSIONS

The effect of the gravity modulation on the natural convection of air and large Prandtl number fluids in a vertical slot with an aspect ratio of 20 and 15, respectively, is studied numerically. We find that the flow enters the periodic state usually after two cycles of modulation for air, while it commonly requires more than 30 cycles to be periodic for large Prandtl number fluids. The response is generally in the synchronous mode, however, it appears to be subharmonic at $\omega_f = 10$ and $R_g = 1$ for air. For a periodic primary flow, we find that the typical convective instability is prone to occur at the nondimensional heights about $y = 1/4$–$1/3$ and $2/3$–$3/4$, instead of around the center as observed in the case of constant gravity. Within the cycle of the gravity modulation, the temperature profile of air is changed significantly. However, the temperature profile of the large Prandtl number fluid is unchanged. We find that the critical temperature gradient at the center has a constant value, approximately 0.56 for $A = 15$, slightly higher than the value obtained in cases without gravity modulation. Although the gravity modulation has a significant effect on the flow patterns in the slot, it shows little effect on the heat transfer rate.

For a multicellular primary flow of air in a slot of $A = 20$, a higher frequency modulation does not appear to stabilize the flow. However, a lower frequency modulation exhibits remarkably stabilizing effect. A large amplitude modulation can make the multicellular flow more vigorous, qualitatively in agreement with the linear stability analysis by Baxi *et al.* [12], while a small amplitude modulation does not show significant stabilizing effect on the flow. The critical Grashof number at parameters $\omega_f = 25$ and $R_g = 1$, with which the gravity modulation notably stabilizes the multicellular primary flow, is found to the $Gr_c^g = 10\,000$–$12\,000$, about 23.6% higher than that with constant gravity.

For the periodically unicellular primary flow of large Prandtl number fluids in a slot of $A = 15$, a new flow pattern is revealed, which consists of two secondary cells aligned in the horizontal direction. This flow pattern develops and emerges periodically during the modulation, and then disappears at the onset of the typical secondary cellular flow consisting

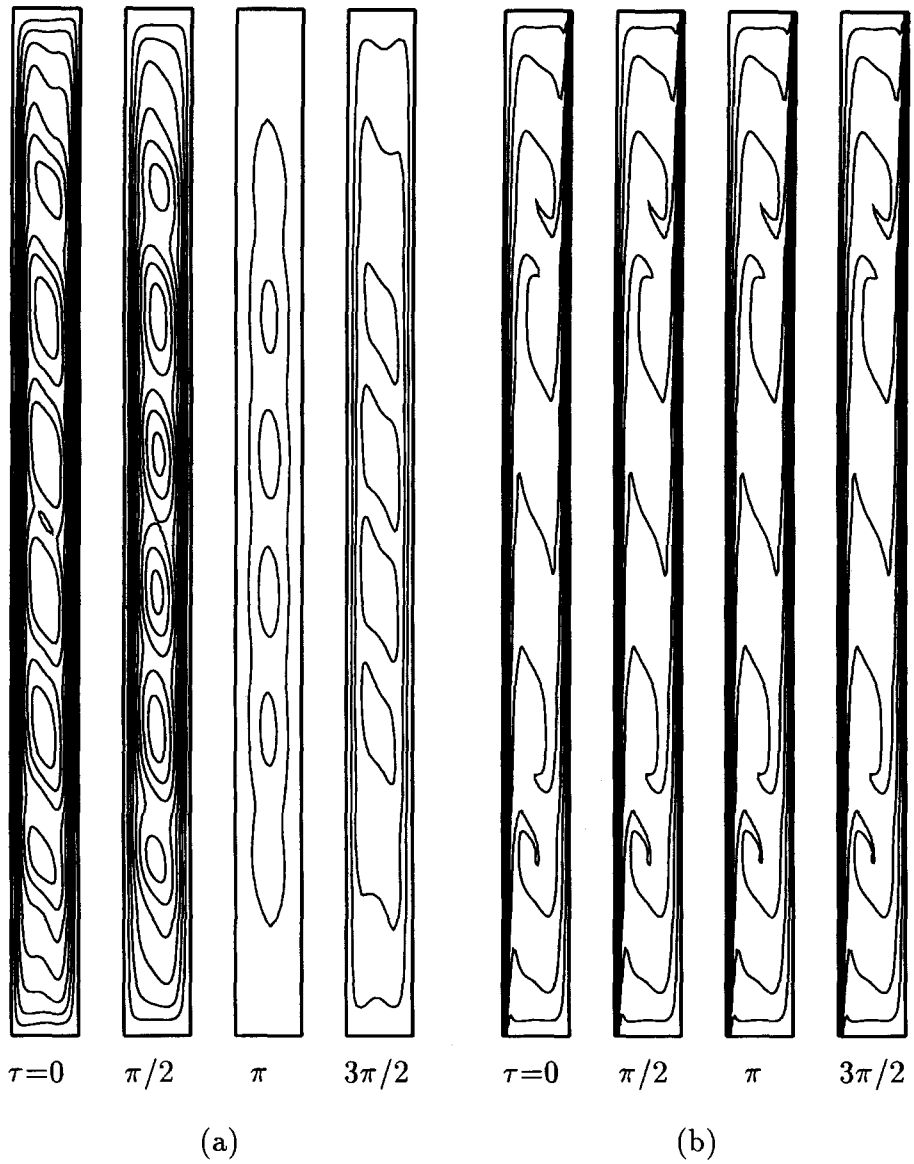

Fig. 16. Flow patterns and isotherms at $Gr = 800$, $Pr = 720$, $\omega_f = 30$ and $R_g = 0.9$ obtained from the multicellular primary flow: (a) flow patterns with $\Delta\psi = 5 \times 10^{-5}$; (b) isotherms.

of cells in the vertical direction. The onset of the secondary flow may be greatly delayed by gravity modulation, depending on the combined effects of the amplitude and frequency of the modulation. It is usually the low frequency that significantly increases the critical Grashof number. For a specific frequency, there seems to be a range of amplitude, in which the stabilizing effect of the gravity modulation is most notable. For $R_g = 0.9$, $\omega_f = 30$ and $R_g = 1.6$, $\omega_f = 40$, we obtained the critical Grashof number $Gr_{cv}^g = 1200$–1400 and 1700–1900, with an increase of approximately 83% and 154%, respectively, compared with the result of constant gravity. Further extensive studies on the combined effects of the amplitude and the frequency of the modulation are obviously necessary.

Acknowledgements—The financial support of NASA Microgravity Science and Application Division through grant NAG3-1386 is gratefully acknowledged.

REFERENCES

1. Nelson, E. S., An examination of anticipated G-jitter on space station and its effects on materials processes. NASA TM 103775, 1991.
2. Gresho, P. M. and Sani, R. L., The effects of gravity modulation on the stability of a heated fluid layer. *Journal of Fluid Mechanics*, 1970, **40**, 783–806.

3. Gershuni, G. Z., Zhukhovitskii, E. M. and Iurkov, I. S., On convective stability in the presence of periodically varying parameter. *Journal of Applied Mathematics & Mechanics*, 1970, **34,** 442–452.
4. Biringen, S. and Danabasoglu, G., Computation of convective flow with gravity modulation in rectangular cavities. *Journal of Thermophysics*, 1990, **4,** 357–365.
5. Biringen, S. and Peltier, J., Numerical simulation of 3-D Benard convection with gravitational modulation. *Physics of Fluids A*, 1990, **2,** 754–764.
6. Clever, R., Schubert, G. and Busse, F. H., Two-dimensional oscillatory convection in a gravitationally modulated fluid layer. *Journal of Fluid Mechanics*, 1993, **253,** 663–680.
7. Ishikawa, M. and Kamei, S., Instabilities of natural convection induced by gravity modulation. *Microgravity Science Technology*, 1994, **4,** 252–259.
8. Saunders, B. V., Murray, B. T., McFadden, G. B., Corriell, S. R. and Wheeler, A. A., The effect of gravity modulation on thermosolutal convection in an infinite layer of fluid. *Physics of Fluids A*, 1992, **4,** 1176–1189.
9. Terrones, G. and Chen, C. F., Convective stability of gravity modulated doubly cross-diffusive fluid layers. *Journal of Fluid Mechanics*, 1993, **225,** 301–321.
10. Ramachandran, N., G-jitter convection in enclosures. *Proceedings of Ninth International Heat Transfer Conference*, Vol. 3. Hemisphere, Washington, DC, 1990, pp. 277.
11. Farooq, A. and Homsy, G. M., Streaming flows due to g-jitter-induced natural convection. *Journal of Fluid Mechanics*, 1994, **271,** 351–378.
12. Baxi, C. B., Arpaci, V. S. and Vest, C. M., Stability of natural convection in an oscillating vertical slot. *Proceedings of the* 1974 *Heat Transfer and Fluid Mechanics Institute*. Stanford University Press, California, 1974, pp. 171–183.
13. Gershuni, G. Z. and Zhukhovitskii, E. M., Convective instability of a fluid in a vibration field under conditions of weightlessness. *Izvestiya Akademii Nauk SSSR, Mekhanika Zhidkosti i gaza*, Vol. 4, 1981, pp. 12–19.
14. Sharifulin, A. N., Stability of convective motion in a vertical layer in the presence of longitudinal vibrations. *Izvestiya Akademii Nauk SSSR, Mekhanika Zhidkosti i gaza*, Vol. 2. 1983, pp. 186–188.
15. Alexander, J. I. D., Amiroudine, S., Quzzani, J. and Rosenberger, E., Analysis of the low gravity tolerance of Bridgman–Stockbarger crystal growth II, transient and periodic accelerations. *Journal of Crystal Growth*, 1991, **113,** 21–38.
16. Bergholz, R. F., Instability of steady natural convection in a vertical fluid layer. *Journal of Fluid Mechanics*, 1978, **84,** 743–768.
17. Lee, Y. and Korpela, A., Multicellular natural convection in a vertical slot. *Journal of Fluid Mechanics*, 1983, **126,** 91–121.
18. Le Quéré, P., A note on multiple and unsteady solutions in two-dimensional convection in a tall cavity. *ASME Journal of Heat Transfer*, 1990, **112,** 965-974.
19. Elder, J. W., Laminar free convection in a vertical slot. *Journal of Fluid Mechanics*, 1965, **23,** 77–98.
20. Lauriat, G. and Desrayaud, G., Natural convection in air-filled cavities of high aspect ratios: discrepancies between experimental and theoretical results. ASME Paper 85-HT-37, 1985.
21. Jin, Y. Y. and Chen, G. F., Instability of convection and heat transfer of high Prandtl number fluids in vertical slot. *ASME Journal of Heat Transfer*, 1996, **118,** 359–365.
22. Chen, F. L. and Wu, C. H., Unsteady convection flows in a vertical slot containing variable viscosity fluids. *International Journal of Heat and Mass Transfer*, 1993, **36,** 4233–4246.
23. Wakitani, S., Experiments on convective instability of large Prandtl number fluids in a vertical slot. *ASME Journal of Heat Transfer*, 1994, **116,** 120–126.
24. Daniels, P. and Wang, P., Numerical study of thermal convection in tall laterally heated cavities. *International Journal of Heat and Mass Transfer*, 1994, **37,** 375–386.
25. Arakawa, A., Computational design for long-term numerical integration of the equations of fluid motion: two dimensional incompressible flow, part I. *Journal of Computational Physics*, 1966, **1,** 119–143.
26. DuFort, E. C. and Frankel, S. P., Stability conditions in the numerical treatment of parabolic differential equations. *Mathematical Tables & Other Aids to Computation*, 1953, **7,** 135–152.
27. Roache, P. J., *Computational Fluid Dynamics*. Hermosa, Albuquerque, NM, 1982.
28. Van Doormaal, J. P. and Raithby, G. D., Enhancement of the SIMPLE method for predicting incompressible fluid flows. *Numerical Heat Transfer*, 1984, **7,** 147–1684.
29. Patankar, S. V., A calculation procedure for two-dimensional elliptic situations. *Numerical Heat Transfer*, 1981, **4,** 409–425.
30. Chen, C. F. and Thangam, S., Convective stability of a variable-viscosity fluid in a vertical slot. *Journal of Fluid Mechanics*, 1985, **161,** 161–173.